nature genetics

Lung regeneration by multipotent stem cells residing at the bronchioalveolar-duct junction

Qiaozhen Liu [1,2,14], Kuo Liu[1,14], Guizhong Cui[1,14], Xiuzhen Huang [1,2], Shun Yao[1], Wenke Guo[1,3], Zhen Qin[1], Yan Li [1,2], Rui Yang[1,2], Wenjuan Pu [1,2], Libo Zhang [1], Lingjuan He [1,2], Huan Zhao[1,2], Wei Yu [1,2], Muxue Tang[1,4], Xueying Tian [5], Dongqing Cai[5], Yu Nie [6], Shengshou Hu[6], Tao Ren[7], Zengyong Qiao[8], Hefeng Huang[9], Yi Arial Zeng[1], Naihe Jing [1,3], Guangdun Peng [1,10,11,12]★, Hongbin Ji [1,3]★ and Bin Zhou [1,2,3,5,12,13]★

Characterizing the stem cells responsible for lung repair and regeneration is important for the treatment of pulmonary diseases. Recently, a unique cell population located at the bronchioalveolar-duct junctions has been proposed to comprise endogenous stem cells for lung regeneration. However, the role of bronchioalveolar stem cells (BASCs) in vivo remains debated, and the contribution of such cells to lung regeneration is not known. Here we generated a genetic lineage-tracing system that uses dual recombinases (Cre and Dre) to specifically track BASCs in vivo. Fate-mapping and clonal analysis showed that BASCs became activated and responded distinctly to different lung injuries, and differentiated into multiple cell lineages including club cells, ciliated cells, and alveolar type 1 and type 2 cells for lung regeneration. This study provides in vivo genetic evidence that BASCs are bona fide lung epithelial stem cells with deployment of multipotency and self-renewal during lung repair and regeneration.

The lung has an elegant architecture composed of trachea, bronchi, bronchioles and alveoli from proximal to distal in anatomy, which is essential for its gas exchange and host defense functions. In the trachea and main bronchi in mice, the lung epithelium consists of ciliated cells, club cells, goblet cells and undifferentiated basal cells, whereas the smaller intralobar bronchioles consist of mainly a layer of ciliated cells, club cells and clusters of neuroendocrine cells that are mostly located at the bronchial branch points[1,2]. The alveolar epithelial cells mainly consist of alveolar type 1 and type 2 (AT1 and AT2) cells[3]. These diverse lung epithelial cells are in direct contact with the outside environment, inhaled particles and pathogens. Once damaged, these epithelial cells must be replaced rapidly to maintain lung structure and function[4]. Cellular mechanisms regulating lung homeostasis and regeneration are not well understood. Understanding the role of lung resident stem or progenitor cells in the maintenance of the airway epithelium during lung homeostasis and repair should provide novel insights into therapeutic approaches for treating pulmonary diseases[5–9]. In accordance with the diversity of cell composition, different epithelial regions and compartments in the lung are maintained and repaired by distinct resident stem-cell populations. Basal cells[10–12], club cells[13,14] and AT2 cells[5,15–17] have been reported to be the main

endogenous stem-cell populations for the lung trachea, bronchi and alveoli, respectively. Moreover, recent studies have indicated more complex and heterogeneous lung-resident stem or progenitor cells. p63+Krt5+ stem cells undergo proliferative expansion in response to influenza-induced lung injuries and differentiate into bronchiolar secretory cells, AT1 and AT2 cells[8,18]. Under special conditions, when basal cells are depleted, committed lung epithelial cells such as club cells can dedifferentiate into basal cells and function as endogenous stem cells, repairing epithelial injury[19]. Recent studies have also reported a stem-cell population termed BASCs that are located at the bronchioalveolar-duct junctions (BADJs) and coexpress club-cell and AT2-cell markers[20,21]. However, the existence of functional BASCs in vivo and their roles during lung repair and regeneration remain controversial.

Club cells in bronchioles express secretoglobin 1a1 (Scgb1a1 or CC10), and AT2 cells in alveoli express surfactant protein C (Sftpc or SPC). The BADJ has been reported as a niche that houses putative BASCs[20] that express both Scgb1a1 and Sftpc[21] (Fig. 1a). Previous studies have mainly used antibody staining, cell isolation and in vitro organoid-culture systems to characterize the molecular profiles and functional properties of BASCs[20–25]. Whether BASCs are an authentic stem-cell population in vivo is not yet known and is under

[1]The State Key Laboratory of Cell Biology, CAS Center for Excellence on Molecular Cell Science, Shanghai Institute of Biochemistry and Cell Biology, University of Chinese Academy of Sciences, Chinese Academy of Sciences, Shanghai, China. [2]Institute of Nutritional Sciences, Shanghai Institutes for Biological Sciences, University of Chinese Academy of Sciences, Chinese Academy of Sciences, Shanghai, China. [3]School of Life Science and Technology, Shanghai Tech University, Shanghai, China. [4]School of Life Sciences, East China Normal University, Shanghai, China. [5]Key Laboratory of Regenerative Medicine of Ministry of Education, Jinan University, Guangzhou, China. [6]State Key Laboratory of Cardiovascular Disease, Fuwai Hospital, National Center for Cardiovascular Disease, Chinese Academy of Medical Sciences and Peking Union Medical College, Beijing, China. [7]Department of Respiratory Medicine, Shanghai Jiao Tong University Affiliated Sixth People's Hospital, Shanghai, China. [8]Department of Cardiovascular Medicine, Southern Medical University Affiliated Fengxian Hospital, Shanghai, China. [9]The International Peace Maternity and Child Health Hospital, School of Medicine, Shanghai Jiao Tong University, Shanghai, China. [10]CAS Key Laboratory of Regenerative Biology and Guangdong Provincial Key Laboratory of Stem Cell and Regenerative Medicine, Guangzhou Institutes of Biomedicine and Health, Chinese Academy of Sciences, Guangzhou, China. [11]Guangzhou Regenerative Medicine and Health Guangdong Laboratory (GRMH-GDL), Guangzhou, China. [12]Institute for Stem Cell and Regeneration, Chinese Academy of Sciences, Beijing, China. [13]Collaborative Innovation Center For Cardiovascular Disease Translational Medicine, Nanjing Medical University, Nanjing, China. [14]These authors contributed equally: Qiaozhen Liu, Kuo Liu, Guizhong Cui. *e-mail: peng_guangdun@gibh.ac.cn; hbji@sibcb.ac.cn; zhoubin@sibs.ac.cn
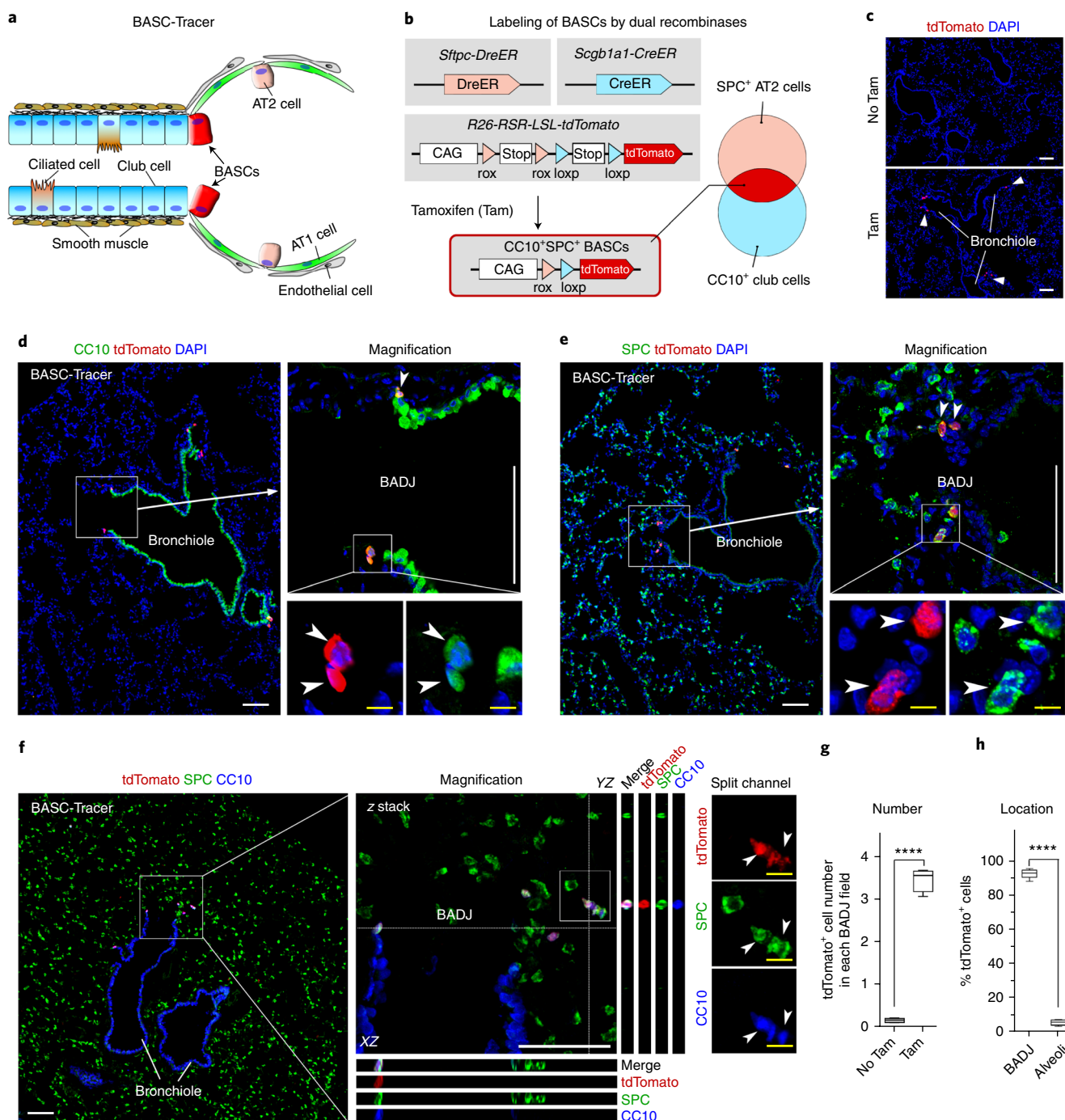
Fig. 1 | Genetic lineage tracing of CC10+SPC+ BASCs with dual recombinases. a, Cartoon image showing the locations of BASCs in the lung. **b**, Illustration of an intersectional genetic lineage-tracing strategy for BASCs, using a BASC-Tracer mouse. **c**, Immunostaining for tdTomato on lung sections of BASC-Tracer mice. **d,e**, Immunostaining for tdTomato and CC10 (**d**) or SPC (**e**) on lung sections of BASC-Tracer mice after tamoxifen induction. Arrowheads indicate tdTomato+CC10+ (**d**) or tdTomato+SPC+ (**e**) BASCs. Images in **d** and **e** are consecutive lung sections. **f**, Immunostaining for tdTomato, CC10 and SPC on a lung section of a BASC-Tracer mouse with tamoxifen induction. *XZ* and *YZ* indicate signals from the dotted line on the *z*-stack image. Arrowheads indicate tdTomato+CC10+SPC+ BASCs. **g**, Quantification of tdTomato+ cell numbers in each BADJ field. **h**, Quantification of the percentage of tdTomato+ cells located in the BADJ or alveoli region. ****$P < 0.0001$, $n = 5$ biologically independent mice; data are shown in box-and-whisker plots; the box spans the interquartile range, the band inside the box represents the median, and whiskers represent the maximum and minimum values; P values were calculated with two-tailed t tests (**g,h**). Scale bars: white, 100 μm; yellow, 10 μm. Each image is a representative of five biologically independent mice (**c**–**f**).

debate, because genetic lineage-tracing studies have suggested that dedicated stem cells rather than putative BASCs are responsible for lung repair and regeneration[13,15]. For instance, club cells are largely responsible for bronchiolar repair, whereas AT2 cells are mainly accountable for alveolar repair[13,15]. Lineage-tracing studies using *Scgb1a1-CreER* or *Sftpc-CreER*, label most club cells or a subset of AT2 cells in addition to BASCs[13,15]. Owing to the lack of genetic tools that specifically target these putative BASCs, the existence of BASCs and their potential roles in lung regeneration after injuries remain unknown and unexplored.

Here we generated a dual lineage-tracing system by using Dre and Cre double recombinase[26,27] to fate-map CC10⁺SPC⁺ BASCs during lung maintenance and after bronchiolar or alveolar injuries. Our genetic lineage-tracing data showed that BASCs became activated and responded distinctly to different lung injuries, and differentiated into multiple cell lineages including club cells, ciliated cells, and AT1 and AT2 cells for lung regeneration. This study provides genetic evidence for the in vivo function of BASCs and their multipotency for lung repair and regeneration.

Results

Generation of a dual-recombinase-mediated lineage-tracing system for BASCs. We first established a genetic lineage-tracing system to specifically track BASCs in vivo. To trace CC10⁺SPC⁺ BASCs (Fig. 1a), we took advantage of a recently developed dual-recombinase-based lineage-tracing system[26,27] to achieve intersectional genetics. Through use of a *Rosa26–rox–Stop–rox–loxP–Stop–loxP–tdTomato* (*R26–RSR–LSL–tdTomato*) reporter[28], we found that only cells coexpressing Dre and Cre (Dre⁺Cre⁺ cells) generated both Dre–*rox* and Cre–*loxP* recombinations, thus leading to the removal of two Stop cassettes and the activation of tdTomato expression (Fig. 1b). Through a *R26–tdTomato* reporter[29], *Scgb1a1–CreER* mainly targeted CC10⁺ club cells in the trachea, bronchi and bronchioles (Supplementary Fig. 1). We treated *Scgb1a1–CreER;R26–tdTomato* mice with 0.025 mg g⁻¹ tamoxifen, and found that more than 70% of CC10⁺ club cells were tdTomato⁺, whereas very few (approximately 0.1%) AT2 cells were tdTomato⁺. Importantly, BASCs could be labeled at this low dosage of tamoxifen (Supplementary Fig. 2). We next generated a *Sftpc–DreER* knock-in mouse (Supplementary Fig. 3a) and crossed it with a *R26–RSR–tdTomato* reporter mouse[30]. *Sftpc–DreER* mainly targeted SPC⁺ AT2 cells and also SPC⁺CC10⁺ BASCs at the BADJs (Supplementary Fig. 3b–h).

We crossed *Sftpc–DreER*, *Scgb1a1–CreER* and *R26–RSR–LSL–tdTomato* mice to generate a triple-knock-in mouse, termed the BASC-Tracer mouse hereafter (Fig. 1a,b). In the BASC-Tracer mouse, tamoxifen treatment induced both Cre–*loxP* and Dre–*rox* recombination simultaneously, thus leading to the expression of the tdTomato reporter in CC10⁺SPC⁺ BASCs (Fig. 1b). By analyzing lungs of BASC-Tracer mice 1 week after 0.025 mg g⁻¹ tamoxifen induction, we found that most tdTomato signals were restricted to BADJ regions (Fig. 1c). Immunostaining for tdTomato and CC10 or SPC on consecutive lung sections showed that these tdTomato⁺ cells expressed CC10 and SPC (Fig. 1d,e). z-stack confocal imaging of BASC-Tracer mouse lung sections triple-stained for tdTomato, CC10 and SPC showed that tdTomato⁺ cells at BADJs were SPC⁺CC10⁺ (Fig. 1f), a result consistent with previous findings[21]. There were 3.45 ± 0.26 tdTomato⁺ cells (462 BADJ fields for five mice, and 15 tissue sections per mouse) residing in each BADJ field (Fig. 1g). Quantitatively, 0.13 ± 0.11% CC10⁻SPC⁺ cells, 0.86 ± 0.43% CC10⁺SPC⁻ cells and 77.16 ± 6.12% CC10⁺SPC⁺ cells in BADJ fields were labeled by tdTomato. BASC-Tracer did not label T1a⁺ alveolar type 1 (AT1) cells, β-tubulin⁺ ciliated cells or CGRP⁺ neuroendocrine cells (Supplementary Fig. 5). Cells labeled in BASC-Tracer mice did not express putative stem/progenitor-cell markers Krt5 (K5) or p63 (Supplementary Fig. 6). *Scgb1a1–CreER* or *Sftpc–DreER* alone did not label lung epithelial cells with the *R26–RSR–LSL–tdTomato* reporter (Supplementary Fig. 7), thus indicating that the tdTomato signals detected in BASC-Tracer mice were the result of dual recombinations controlled by both Cre and Dre. We also examined the lungs of BASC-Tracer mice without tamoxifen treatment. In most fields, we did not detect any tdTomato signal (Supplementary Fig. 8a). Only rarely did we detect single tdTomato⁺ cells that were located at the BADJ and coexpressed SPC and CC10 but not T1a (Supplementary Fig. 8b,c). Quantification data confirmed that the tdTomato⁺ cell numbers (0.15 ± 0.047 tdTomato⁺ cells per BADJ field, counted from 425 BADJ fields for five mice, 15 tissue sections

per mouse) were negligible in BASC-Tracer mice without tamoxifen treatment compared with the tamoxifen-treated group (Fig. 1g). Notably, 92.80 ± 2.65% of tdTomato⁺ cells were located in the BADJ regions, whereas 5.38 ± 1.51% of tdTomato⁺ cells were located in the alveolar region (Fig. 1h), thus suggesting that most labeled cells were BASCs at the BADJ region. Together, these results demonstrated that we established a genetic lineage-tracing system that can be used to specifically target and trace BASCs in vivo.

Fate-mapping of BASCs during lung homeostasis. We next traced BASCs cell fate during lung homeostasis by collecting BASC-Tracer mouse lungs at 1, 2 and 3 weeks (short term) or 12 and 24 weeks (long term) after tamoxifen treatment (Fig. 2a). We found that tdTomato⁺ cells remained at BADJs after 12 weeks (Fig. 2b). Immunostaining for tdTomato and CC10 or SPC showed that tdTomato⁺ cells in BASC-Tracer mouse lungs expressed CC10 or SPC (Fig. 2c). Quantification of the number of tdTomato⁺ cells at each BADJ showed that the number of tdTomato⁺ cells increased from 3.45 ± 0.26 cells at baseline to 4.72 ± 0.48 cells after 12 weeks and 5.53 ± 0.39 cells after 24 weeks during homeostasis (389 BADJ fields for five mice, 15 tissue sections per mouse, Fig. 2d,i), thus indicating that tdTomato⁺ cells expanded after 12 or 24 weeks (Fig. 2i). However, the tdTomato⁺ cells at BADJs were not necessarily CC10⁺SPC⁺ BASCs after long-term tracing, because tdTomato⁺ cells may include not only CC10⁺SPC⁺ BASCs but also their descendants that do not continue to exhibit CC10⁺SPC⁺ double positivity. We therefore triple-stained CC10, SPC and tdTomato in lung tissue sections of BASC-Tracer mice to quantify the number of tdTomato⁺CC10⁺SPC⁺ BASCs (Fig. 2d–h). After a 12-week chase period, most tdTomato⁺ cells still maintained CC10 and SPC double positivity (Fig. 2f), but we also detected some tdTomato⁺CC10⁺SPC⁻ and tdTomato⁺CC10⁻SPC⁺ cells (Fig. 2g). Quantification results showed that the percentage of CC10⁺SPC⁺ cells in the tdTomato⁺ cell population decreased while the percentage of CC10⁺SPC⁻ or CC10⁻SPC⁺ cells in the tdTomato⁺ cell populations adjacent to BADJ fields increased from 1 week to 12 weeks after tamoxifen induction (Fig. 2e,g), thus indicating that some BASCs lost SPC or CC10 expression during lung homeostasis and converted into CC10 or SPC single-positive cells, respectively (Fig. 2g). In addition, we found that the tdTomato⁺CC10⁺SPC⁺ BASCs number did not change significantly between 1 week (3.36 ± 0.48, counted from 124 BADJ fields for five mice, 12 tissue sections per mouse), 12 weeks (3.59 ± 0.30, counted from 118 BADJ fields for five mice, 12 tissue sections per mouse) and 24 weeks (3.46 ± 0.31, 146 BADJ fields for five mice, 12 tissue sections per mouse) after tamoxifen induction (Fig. 2h). To rule out the possibility that the expansion of tdTomato⁺ cells might have been a result of a residual tamoxifen effect[31], we also collected BASC-Tracer lungs 2 and 3 weeks after induction and examined their labeling efficiency. Quantification data showed that tdTomato⁺ cells per BADJ filed were 3.45 ± 0.26, 3.34 ± 0.31 and 3.71 ± 0.30 at 1, 2 and 3 weeks, respectively (Fig. 2i), thus indicating no significant changes, excluding the putative tamoxifen residual effect. During lung homeostasis, BASCs rarely gave rise to AT1 cells (Fig. 2j). Together, these data demonstrated that the number of BASCs is relatively stable level during lung homeostasis (Fig. 2k).

BASCs give rise to club cells and ciliated cells after bronchiolar injury. To understand the roles of BASCs in lung repair and regeneration after injuries, we first generated a bronchiolar-injury model through naphthalene exposure, which depleted club cells in bronchioles[20]. Adult BASC-Tracer mice were treated with tamoxifen at an age of 7 weeks and then subjected to naphthalene or vehicle (corn oil) treatment 1 week after tamoxifen induction (Fig. 3a). We found bronchiole-like tdTomato signal patterns in the naphthalene-treated mice (Fig. 3b,c). BASCs contributed significantly to CC10⁺ club cells and regenerated terminal bronchioles (Fig. 3d). We did
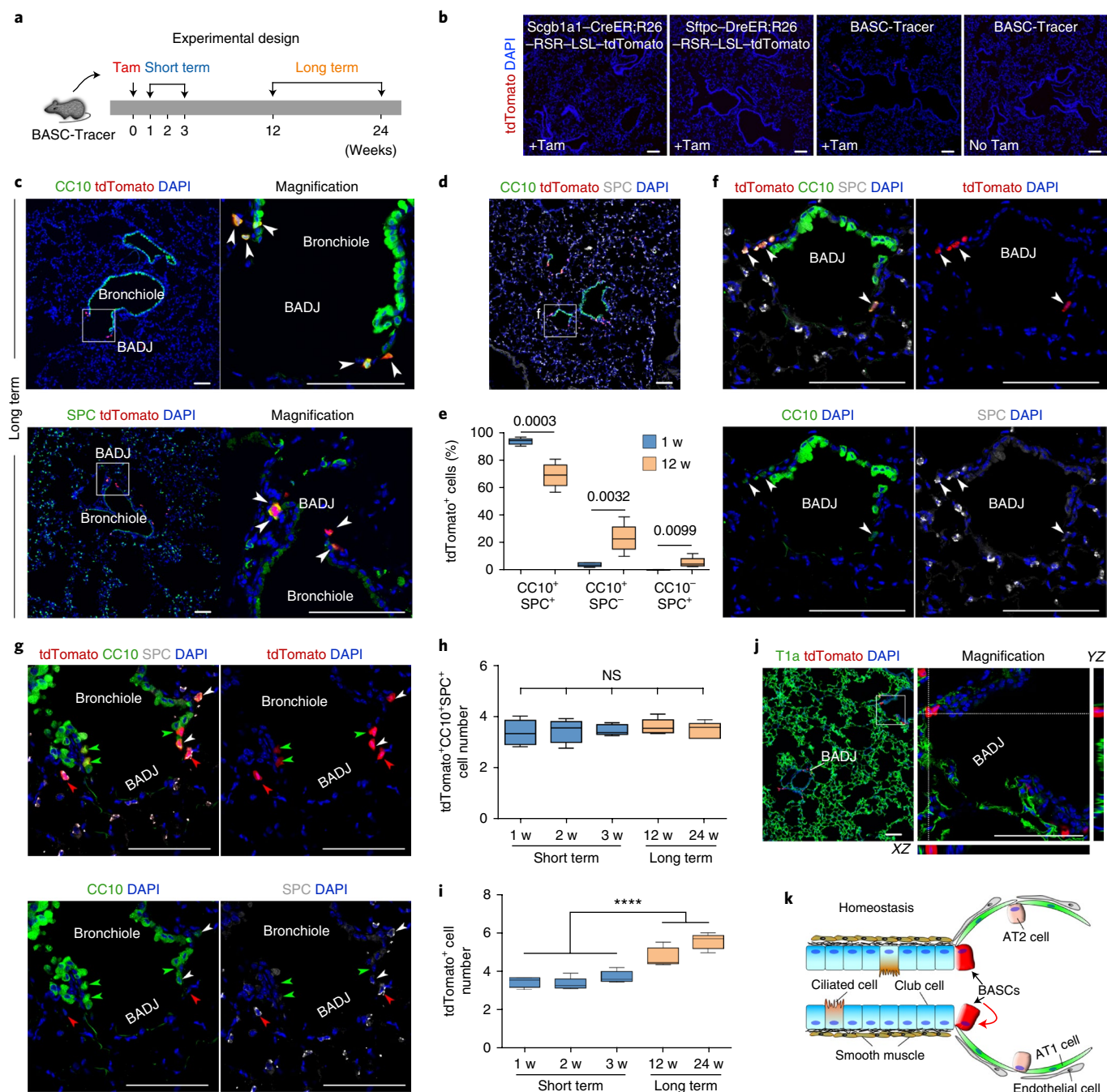
Fig. 2 | Maintenance of BASCs during lung homeostasis. a, Schematic showing experimental design. Samples were analyzed after short-term or long-term tracing. Tam, tamoxifen. **b**, Immunostaining for tdTomato on lung sections shows the specificity of BASC-Tracer in cell labeling; littermate controls of different genotypes are shown. **c**, Immunostaining for tdTomato and CC10 or SPC on lung sections of BASC-Tracer mice 12 weeks after tamoxifen induction. Arrowheads indicate tdTomato⁺CC10⁺ or tdTomato⁺SPC⁺ cells in BADJ regions. **d**, Triple staining for tdTomato, CC10 and SPC on lung sections of BASC-Tracer mice 12 weeks after tamoxifen induction (12 w). Boxed regions are magnified in **f. e**, Quantification of the percentage of CC10⁺SPC⁺ cells, CC10⁺SPC⁻ cells and CC10⁻SPC⁺ cells in tdTomato⁺ cells. *P* values are indicated in the figure and are derived from a two-tailed *t* test. **f,g**, White arrowheads indicate tdTomato⁺CC10⁺SPC⁺ cells; red arrowheads indicate tdTomato⁺CC10⁻SPC⁺ cells; green arrowheads indicate tdTomato⁺CC10⁺SPC⁻ cells. **h,i**, Quantification of the number of tdTomato⁺CC10⁺SPC⁺ BASCs (**h**) or tdTomato⁺ cells (**i**) in each BADJ field. NS, not significant, *P* = 0.8999, one-way analysis of variance (**h**); ****P* < 0.0001, two tailed *t* test (**i**), *n* = 5 biologically independent mice; data are shown in box-and-whisker plots; the box spans the interquartile range, the band inside the box represents the median, and the whiskers represent maximum and minimum values (**e,h-i**). **j**, Immunostaining for T1a and tdTomato on lung sections 12 weeks after tamoxifen induction. *XZ* and *YZ* indicate signals from the dotted line on the z-stack image. **k**, Cartoon image showing maintenance of BASCs in lung homeostasis. Scale bars, 100 μm. Each image is representative of five individual biological samples.

not detect a significant contribution of BASCs to SPC⁺ AT2 cells in the naphthalene-treated mice compared with the vehicle group (Fig. 3e). In the vehicle group, tdTomato⁺ cells still remained at BADJs, expressing CC10 and SPC (Fig. 3d,e). Quantification data

showed a significant increase in bronchiolar tdTomato⁺CC10⁺ cell number (the height of tdTomato⁺ club-cell strand in the bronchiole) in naphthalene-treated mice compared with vehicle controls (20.27 ± 1.88 naphthalene versus 1.70 ± 0.36 vehicle; counted from
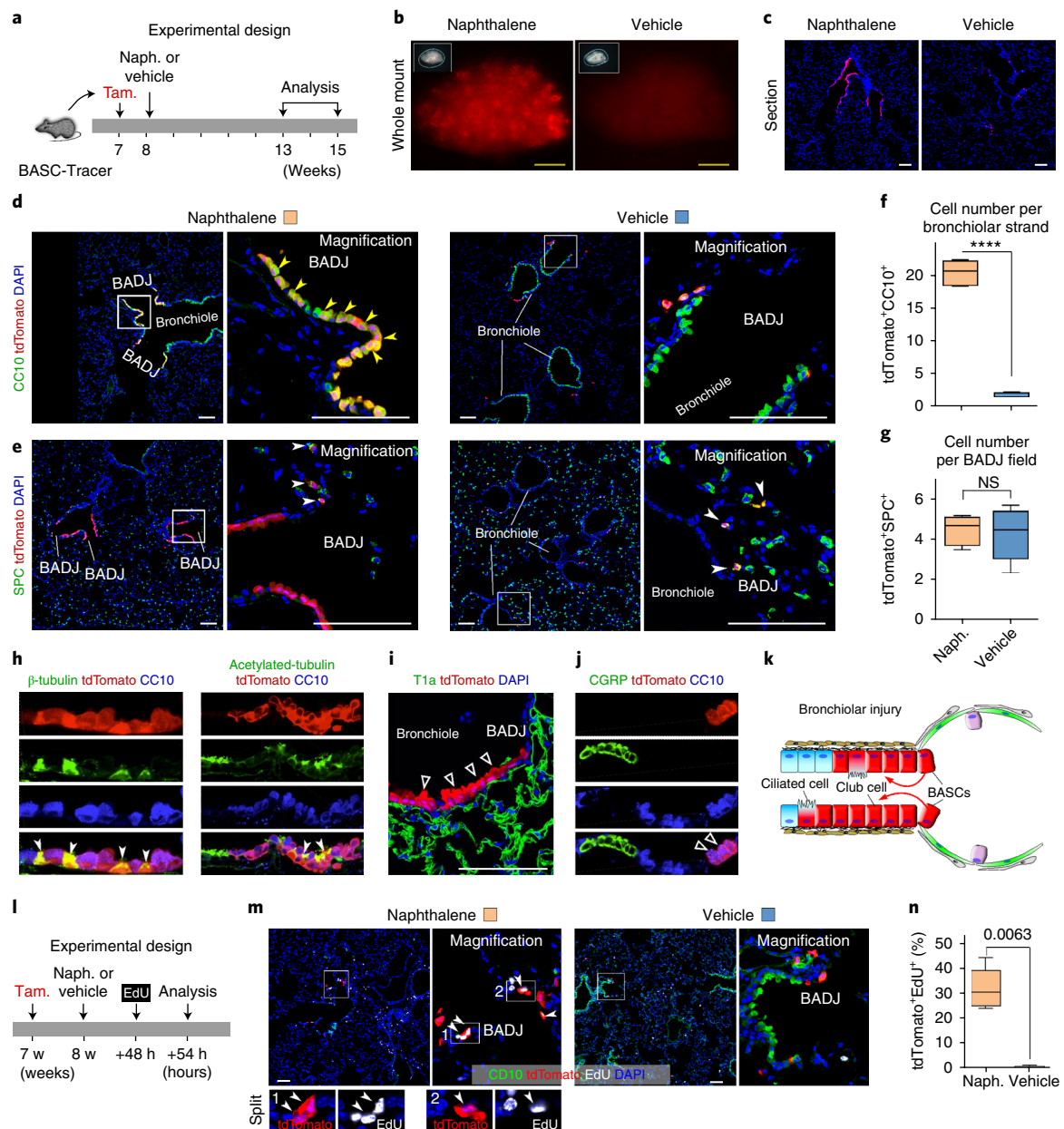
Fig. 3 | BASCs contribute to club cells and ciliated cells after bronchiolar injury. a, Schematic figure showing a timeline for tamoxifen, naphthalene (Naph.) or corn oil (vehicle) treatment, and lung tissue analysis. **b**, Whole-mount bright-field or fluorescence images of BASC-Tracer mouse lungs after naphthalene or vehicle treatment. **c**, Immunostaining for tdTomato on lung sections, showing expansion of BASCs after injury. **d,e**, Immunostaining for tdTomato and CC10 (**d**) or SPC (**e**) on lung sections after naphthalene or vehicle treatment. Yellow arrowheads indicate CC10+ cells derived from tdTomato+ BASCs; white arrowheads indicate SPC+ cells in BADJ. **f,g**, Quantification of the tdTomato+CC10+ cell number in each bronchiolar strand (**f**) or tdTomato+SPC+ cell number in each BADJ field (**g**). ****$P < 0.0001$; NS, not significant ($P = 0.052$); two-tailed t test. **h–j**, Immunostaining for tdTomato and β-tubulin, acetylated-tubulin, T1a or CGRP on naphthalene-treated lung sections. BASCs differentiate into β-tubulin+ or acetylated-tubulin+ ciliated cells (**h**) but not T1a+ AT1 cells (**i**) or CGRP+ neuroendocrine cells (**j**). **k**, Diagram showing that BASCs regenerate terminal bronchiole after naphthalene injury. **l**, Schematic showing experimental design. **m**, Immunostaining for CC10, tdTomato and EdU in lung tissue sections. Most CC10+ cells are ablated shortly after naphthalene treatment. White arrowheads indicate tdTomato+EdU+ cells in naphthalene-treated lung tissue. **n**, Quantification of the percentage of tdTomato+ cells with incorporated EdU. $P = 0.0063$; two tailed t test, $n = 5$ biologically independent mice; data are shown in box-and-whisker plots; the box spans the interquartile range, the band inside the box represents the median, and whiskers represent the maximum and minimum values (**f,g,n**). Scale bars: yellow, 2 mm; white, 100 μm. Each image is representative of five individual samples.

234 and 198 BADJ fields, respectively, in five mice, 15 tissue sections per mouse; Fig. 3f). In contrast, the tdTomato+SPC+ cell number per BADJ field did not change significantly (4.76 ± 0.73 naphthalene versus 4.50 ± 1.28 vehicle; counted from 258 and 240 BADJ fields, respectively, in five mice, 15 tissue sections per mouse; Fig. 3g). Triple staining for CC10, SPC and tdTomato on lung tissue sections

validated that most tdTomato+ cells adopted a CC10+SPC− club-cell fate in the terminal bronchioles (Supplementary Fig. 9). Interestingly, BASCs also contributed to β-tubulin+ or acetylated-tubulin+ ciliated cells in terminal bronchioles (Fig. 3h), but not T1a+ AT1 cells or CGRP+ neuroendocrine cells in the injured lung (Fig. 3i,j). These data demonstrated that BASCs differentiate into

club cells and ciliated cells in terminal bronchioles, but not AT1 or AT2 cells in alveoli after naphthalene-induced bronchiolar injury (Fig. 3k). Next we analyzed lungs 54 h after injury with ethynyl deoxyuridine (EdU) injected 6 h before collection to examine the proliferation of BASCs shortly after naphthalene treatment (Fig. 3l). We found that most club cells were depleted after naphthalene treatment, whereas the naphthalene-resistant BASCs still survived and remained at the BADJ (Fig. 3m). The EdU-incorporation assay showed that $31.42 \pm 8.03\%$ of BASCs (counted from 149 BADJ fields respectively in five mice, 12 tissue sections per mouse) were EdU$^+$ 2 d after naphthalene treatment, and scarcely any EdU$^+$ BASCs were detected in the vehicle group (Fig. 3m,n). We excluded putative tamoxifen residual effects by induction of naphthalene 3 weeks after tamoxifen treatment (Supplementary Fig. 10). These data demonstrated that BASC populations are resistant to naphthalene toxin and proliferate substantially after bronchiolar injury, thereby giving rise to club cells and ciliated cells, regenerating the terminal bronchioles.

BASCs contribute to AT1 and AT2 cells after alveolar injury. We next used a lung alveolar-injury model induced by bleomycin to examine the ability of BASCs to regenerate the alveoli. Mice were intratracheally instilled with bleomycin or vehicle (PBS) 1 week after tamoxifen treatment, and lungs were collected approximately 2 months after injury (Fig. 4a). In the bleomycin-treated lung parenchyma, in contrast to the vehicle group, tdTomato$^+$ cell clusters were readily detected (Fig. 4b,c). Immunostaining for tdTomato and cell-lineage markers showed that these tdTomato$^+$ cells were largely squamous AT1 cells and cuboidal AT2-cell clusters, which were distributed near the BADJs and displayed alveolar but not bronchiolar structure (Fig. 4d–f). In the vehicle group, tdTomato$^+$ cells did not contribute significantly to AT1 or AT2 cells, and they mostly retained their BASCs identities, expressing CC10 and SPC (Fig. 4d–f). Quantification of the number of tdTomato$^+$ AT2, AT1 and club cells in each BADJ field showed that BASCs contributed significantly to AT2 and AT1 cells, but not the club cells after bleomycin-induced injury (Fig. 4g–i). Our data showed that 20.81 ± 2.08 versus 5.44 ± 0.69 SPC$^+$tdTomato$^+$ cells (Fig. 4g); 16.06 ± 0.69 versus 0.09 ± 0.067 T1a$^+$tdTomato$^+$ cells (Fig. 4h); 5.06 ± 0.83 versus 3.88 ± 1.16 CC10$^+$tdTomato$^+$ cells (Fig. 4j) were detected in the bleomycin and vehicle groups, respectively (five mice per group). We next collected lung tissues 2.5 weeks after bleomycin or vehicle instillation and injected EdU 24 h before tissue collection (Supplementary Fig. 11a). In contrast to the vehicle group, in the bleomycin-treated group, the lungs exhibited significantly more EdU$^+$ cells (Supplementary Fig. 11b,c). We detected small tdTomato$^+$ cell clusters at the BADJs 2.5 weeks after bleomycin treatment, and a subset of tdTomato$^+$ cells contained EdU incorporation ($5.6 \pm 1.36\%$ versus $0.24 \pm 0.17\%$ of tdTomato$^+$ cells were EdU$^+$ in the bleomycin and vehicle groups, respectively, Fig. 4k,l). We detected EdU$^+$tdTomato$^+$ AT1 and AT2 cells, but not EdU$^+$tdTomato$^+$ club cells in the bleomycin-treated lungs (Supplementary Fig. 11d–f). In the vehicle group, tdTomato$^+$ cells remained at the BADJs and expressed CC10 and SPC but not T1a (Supplementary Fig. 11d–f). There were sparse tdTomato$^+$EdU$^+$ cells in the vehicle group (Fig. 4l). The tdTomato$^+$ AT2 cells in bleomycin-injured lung tissue were CC10$^-$SPC$^+$, thus indicating that the BASCs had fully differentiated into the AT2-cell lineage and had lost CC10 expression (Supplementary Fig. 11g). Bleomycin also induced lung fibrosis with fibroblast cell enrichment (Supplementary Fig. 12a), a result consistent with previous findings[32]. Immunostaining for tdTomato and cell lineage markers showed that BASCs did not contribute to any fibroblasts, pericytes, smooth muscle cells or endothelial cells in the injured lung (Supplementary Fig. 12b–g). We confirmed the above result by induction of bleomycin 3 weeks after tamoxifen treatment (Supplementary Fig. 13). Together, the above results demonstrated that BASCs were activated to expand and differentiate into alveolar cell lineages, such as AT1 and AT2 cells, in response to severe alveolar damage (Fig. 4m).

Genetic clonal analysis of single BASCs after lung injury. To study the single-cell expansion and differentiation behavior of BASCs after lung injury, we generated a multicolor fluorescence-reporter line based on a previously documented confetti reporter[33]. This new reporter (*R26–Confetti2*) contained *rox–Stop–rox* cassettes before confetti, so that only after dual Dre–*rox* and Cre–*loxP* recombination could single-color fluorescence reporters such as yellow fluorescent protein (YFP), green fluorescent protein (GFP) and red fluorescent protein (RFP) be expressed in Dre$^+$Cre$^+$ cells and their descendants (Fig. 5a,b). We generated *Sftpc–DreER;Scgb1a1–CreER;R26–Confetti2* triple-knock-in mice and treated them with tamoxifen for clonal analysis before and after injury (Fig. 5a,b). One week after a single dose of tamoxifen treatment, single BASCs were detected at BADJ, and the labeling was very sparse (Fig. 5c). After naphthalene treatment, we detected a ribbon of CC10$^+$ cells mixed with ciliated cells in single fluorescent color in the terminal bronchioles (Fig. 5d and Supplementary Fig. 14a). Quantification of the fluorescent cells showed that single BASCs contributed significantly to CC10$^+$ club cells after bronchiolar injury, as compared with the vehicle control (Fig. 5e and Supplementary Fig. 14b,c). In the alveolar-injury model, single BASCs expanded substantially and contributed to both SPC$^+$ AT2 and T1a$^+$ AT1 cells, as compared with the vehicle control (Fig. 5f,g and Supplementary Fig. 14d,e). These in vivo clonal fate-mapping data demonstrated that BASCs, at the single-cell level, have multipotency to differentiate into either bronchiolar or alveolar epithelial-cell lineages after different lung injuries.

Single-cell RNA-sequencing analysis identifies BASC markers. To profile the BASC gene expression signature, we performed single-cell RNA sequencing (scRNA-seq) of individual BASCs and compared the results with those for club cells and AT2 cells. Single tdTomato$^+$ epithelial cells were sorted from three groups of mice through a live CD45$^-$CD31$^-$Epcam$^+$tdTomato$^+$ sorting strategy including BASCs-tdTomato (TD) cells from BASC-Tracer mice, Scgb1a1-TD cells from *Scgb1a1–CreER;R26–tdTomato* micse and Sftpc-TD cells from *Sftpc–DreER;R26–RSR–tdTomato* mice (Fig. 6a). Four hundred and eighty single cells were sequenced (160 cells per group), and *t*-distributed stochastic neighbor embedding (*t*-SNE) analysis showed that the isolated cells grouped into four clusters (Fig. 6b). On the basis of the expression of known markers within a particular cell type[18,34,35], the four clusters were assigned as AT2 cell, BASC, club cell and ciliated cell (Fig. 6b–d and Supplementary Fig. 15a,b). By tracking the sources of cells (tdTomato$^+$), we found that BASC-TD cells were mainly located in the BASC cluster, and very few were found in the club-cell and AT2-cell clusters, results consistent with the above immunostaining and quantification results (Fig. 6b,c and Fig. 2e). Sftpc-TD cells were predominantly located in AT2-cell cluster, and a few were observed in the BASCs cluster, but none were observed in the club or ciliated-cell clusters, findings also corroborating the previous immunostaining and quantification results (Fig. 6b,c and Supplementary Fig. 4). Scgb1a1-TD cells were scattered mostly in the club-cell population, and a subset was found in the BASC and ciliated-cell clusters (Fig. 6b,c). BASC-cluster cells expressed the AT2 marker *Sftpc* and club-cell marker *Scgb1a1* (whose expression was lower than that in club cells), but did not express the ciliated-cell marker *Foxj1* (Fig. 6d). We also identified signature genes for each of these cell clusters (Fig. 6e and Supplementary Fig. 15b). Heat-map analysis using cluster signature genes confirmed that the gene profiles of BASCs partly overlapped with that of AT2 and club cells, but not ciliated cells (Fig. 6e). Among the identified putative cluster-specific markers, *Lrg1* and *Plin2* were highly enriched in BASCs (Fig. 6f,g and Supplementary Fig. 15c,d). Expression of *Lrg1* in BASCs suggested that BASCs might participate in lung idiopathic fibrosis[36] and angiogenesis[37]. *Plin2*, also called adipophilin or ADrP, has been reported to be expressed in lung lipofibroblasts and to be important for the synthesis of surfactant phospholipid by AT2
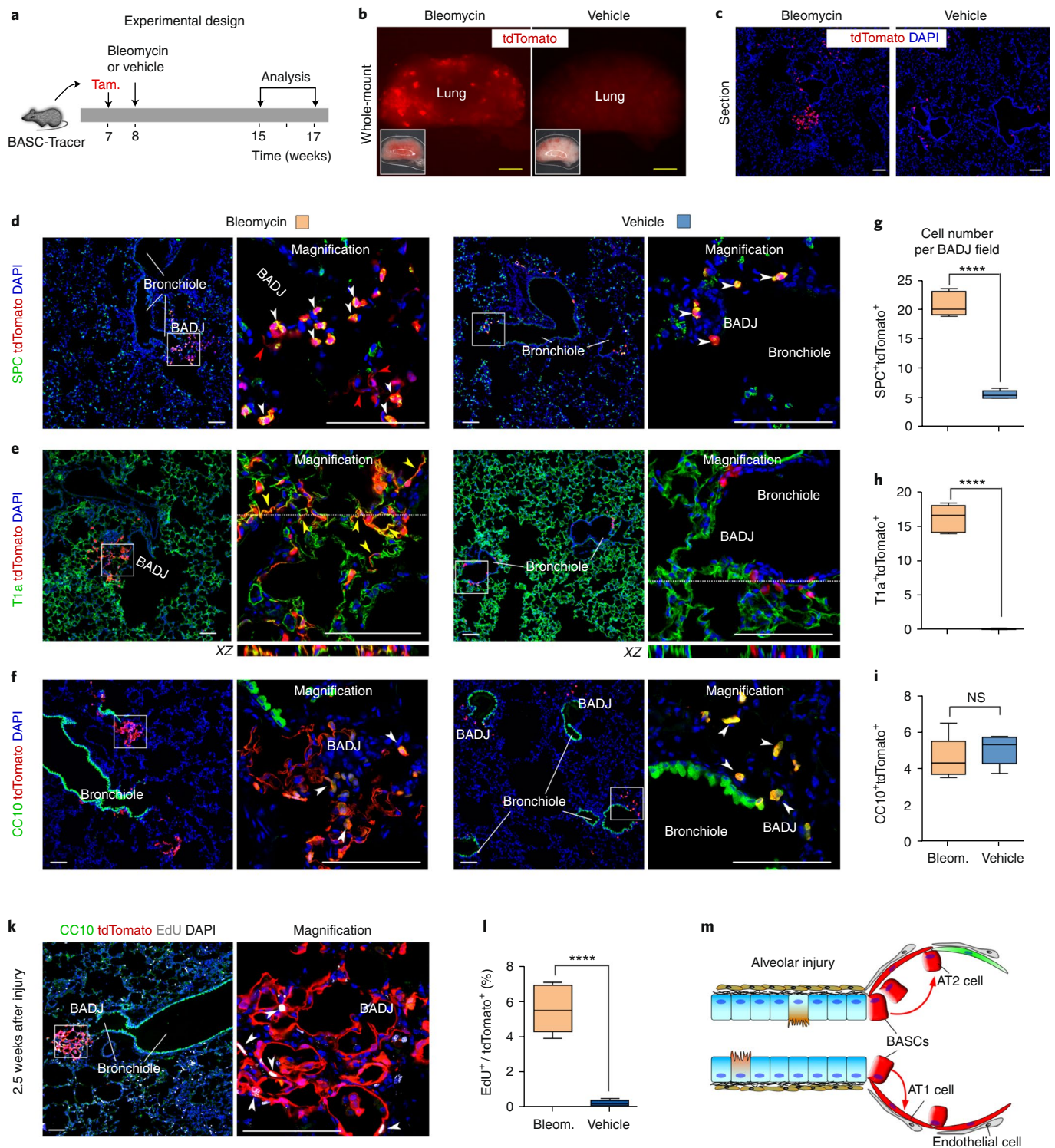
Fig. 4 | BASCs expand and differentiate into AT1 and AT2 cells after bleomycin-induced lung injury. a, Schematic showing experimental design.
b, Whole-mount fluorescence images of lungs from bleomycin or vehicle (PBS) treated BASC-Tracer mice. Insets indicate bright-field images.
c, Immunostaining for tdTomato in lung sections, showing expansion of tdTomato+ cells in the alveoli after injury. **d**, Immunostaining for SPC and tdTomato
on lung tissue sections. White arrowheads indicate SPC+tdTomato+ AT2 cells; red arrowheads indicate SPC–tdTomato+ AT1 cells. **e**, Immunostaining
for T1a and tdTomato on lung sections. *XZ* indicates signals from the dotted line on the *z*-stack image. Yellow arrowheads indicate T1a+tdTomato+ AT1
cells. **f**, Immunostaining for CC10 and tdTomato in lung sections. Arrowheads indicate CC10+tdTomato+ cells. **g–i**, Quantification of SPC+tdTomato+
(**g**), T1a+tdTomato+ (**h**) and CC10+tdTomato+ (**i**) cells in each BADJ field in bleomycin- (Bleom.) or vehicle-treated lung tissues. ****$P < 0.0001$; NS, not
significant ($P = 0.4351$); two-tailed *t* test. **k**, Immunostaining for CC10, tdTomato and EdU on lung tissue section 2.5 weeks after injury. Arrowheads indicate
EdU+tdTomato+ cells. **l**, Quantification of the percentage of tdTomato+ cells with incorporated EdU in each BADJ field; ****$P < 0.0001$. $n = 5$ biologically
independent mice; data are shown in box-and-whisker plots, the box spans the interquartile range, the band inside the box represents the median, and
whiskers represent the maximum and minimum values (**g–i**, **l**). **m**, Diagram showing that BSACs regenerate AT1 and AT2 cells after bleomycin injury.
Scale bars: yellow, 2 mm; white, 100 μm. Each image is representative of five individual samples.
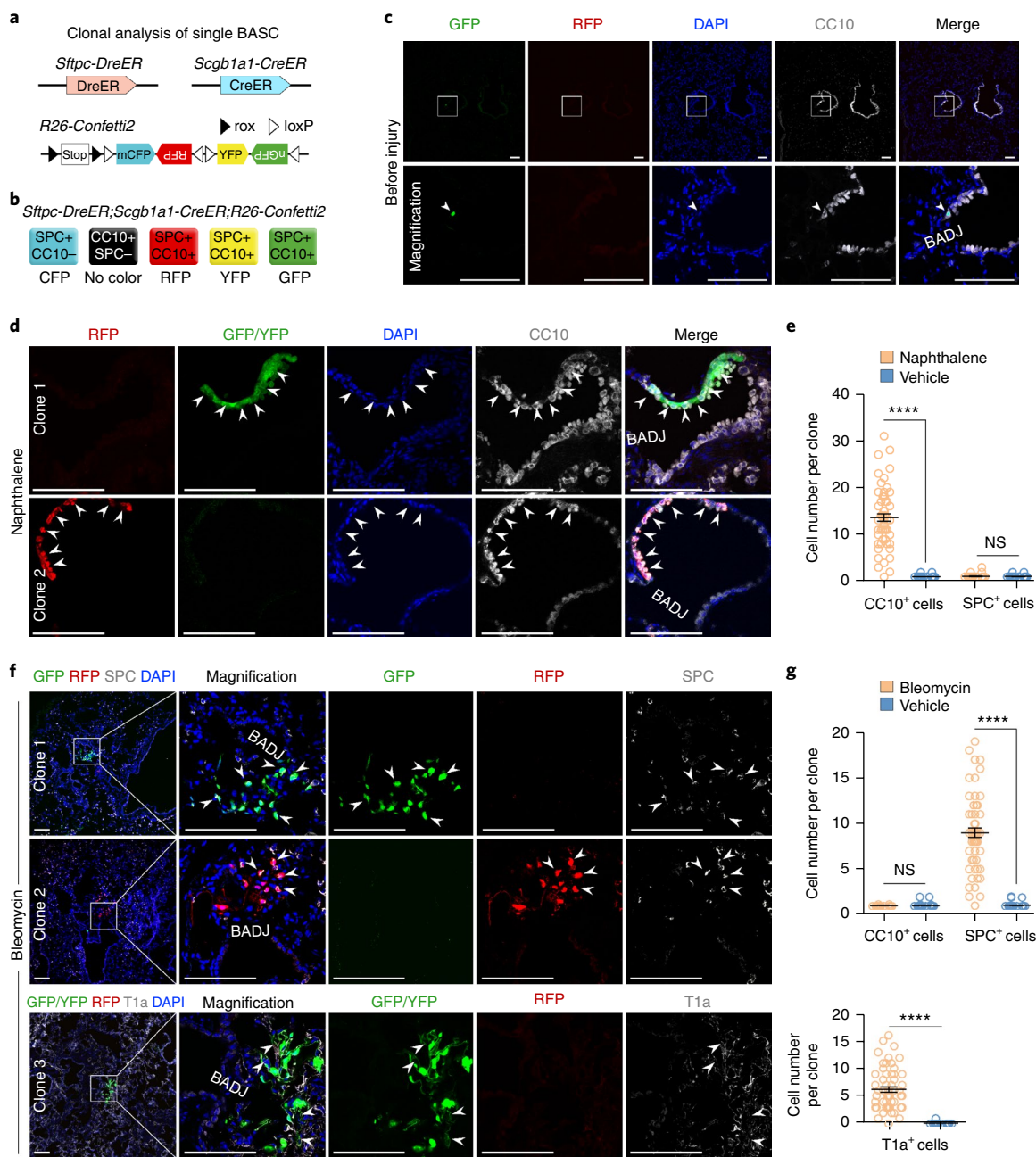
Fig. 5 | Clonal analysis of BASCs in naphthalene- or bleomycin-induced lung injuries. a,b, Schematic showing labeling of single BASCs through generation of a *R26–Confetti2* reporter mouse crossed with a *Sftpc–DreER* and *Scgb1a1–CreER* mouse. Single BASCs were marked by RFP, YFP or GFP after both Dre–rox and Cre–loxP recombination. **c,** Sparse labeling of single fluorescent BASCs (arrowhead) before injury. **d,** Immunostaining for fluorescent proteins and CC10 on lung sections after naphthalene treatment. Arrowheads indicate fluorescent CC10+ cells, and cells in one color (e.g., GFP, YFP or RFP) close to BADJ were regarded as one clone derived from a single BASC. **e,** Quantification of CC10+ or SPC+ cell number in fluorescent clones. Cells labeled by one fluorescent signal indicated one clone. ****$P < 0.0001$; NS, not significant ($P = 0.2952$); two-tailed *t* test. **f,** Immunostaining for fluorescent proteins and SPC (clone 1, 2) or T1a (clone 3) on lung sections after bleomycin treatment. Arrowheads indicate fluorescent SPC+ cells (clone 1, 2) or T1a+ cells (clone 3). **g,** Quantification of CC10+, SPC+ or T1a+ cell number in fluorescent clones. ****$P < 0.001$; NS, not significant ($P = 0.6511$); two-tailed *t* test. Circles represent the cell number in each quantified clone from four biologically independent mice; black bars show mean and error bars indicate s.e.m. (**e,g**). Scale bars, 100 μm. Each image is representative of four individual samples.

cells[38,39]. *PLIN2* is also upregulated in human lung adenocarcinoma compared with normal lung tissue[40], and it is a potential diagnostic marker for lung adenocarcinoma[41]. Enriched expression of *Plin2* in BASCs may indicate the role of BASCs in the progression of lung cancer[21,42,43] under pathological conditions or injury. Further analysis of the BASC population showed that the BASCs could be partitioned into two subpopulations, BASC-1 and BASC-2 (Fig. 6h–j and Supplementary Fig. 15e–h). Together, our scRNA-seq analysis

results showed that BASCs are a transcriptomically distinct population located between the populations of AT2 and club cells. BASCs are heterogeneous and can be partitioned into subpopulations.

Discussion
In this study, we established a genetic lineage-tracing system that specifically labels CC10+SPC+ BASCs at BADJ regions, providing a valuable genetic tool for understanding the in vivo
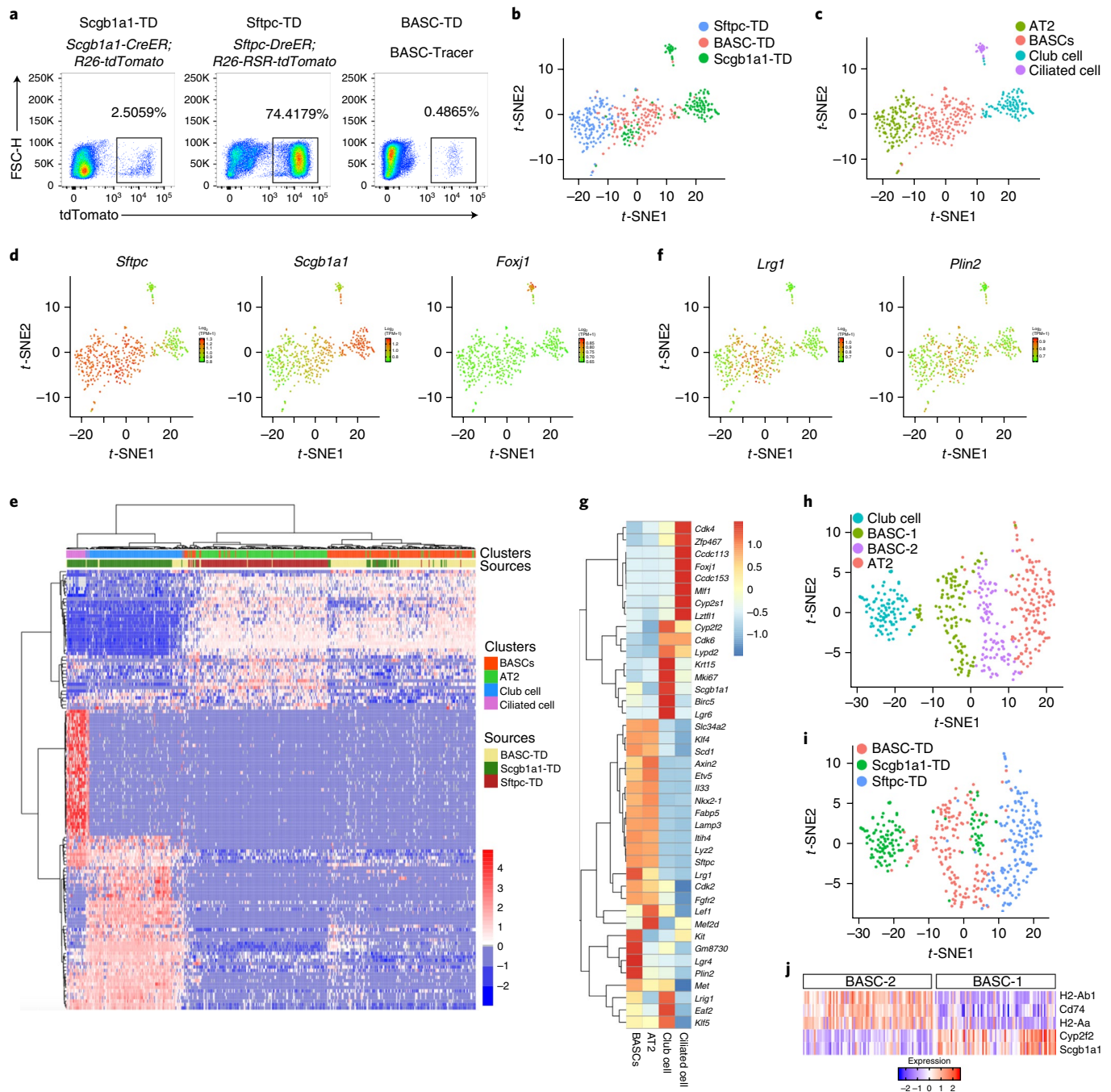
Fig. 6 | Single-cell RNA sequencing of BASCs. a, FACS sorting of tdTomato+ epithelial cells from three groups of mice after tamoxifen treatment; the sorted cells (160 cells per group) are named as Scgb1a1-TD, Sftpc-TD and BASC-TD populations. Representative plot from five independent experiments. **b,c**, *t*-SNE plot of 480 single cells isolated in **a**; cells are colored by tdTomato sources (**b**) or cell-cluster assignment (**c**). **d**, *t*-SNE of 480 scRNA-seq profiles (points) colored by expression (log$_2$(TPM + 1)) of representative AT2-cell, club-cell and ciliated-cell markers. **e**, Heat map and clustering of different expressed genes in the four clusters. **f**, *t*-SNE of 480 scRNA-seq profiles (points) colored by expression (log$_2$(TPM + 1)) of genes highly enriched in the BASC population. **g**, Heat map showing relative average expression of representative genes within the cell cluster. **h, i**, *t*-SNE plot of 455 scRNA-seq profiles (points) without ciliated-cell population; cells were assigned colors according to cell type (**h**) or tdTomato source (**i**). BASCs can be clustered into two subpopulations (**h**). **j**, Heat map showing genes differently expressed in the two BASC subpopulations (log$_2$(TPM + 1), 0.5 > FC > 2).

function of BASCs during lung homeostasis and after injury. We found that the number of BASCs expressing both CC10 and SPC remains stable during lung homeostasis. After bronchiolar or alveolar injury, BASCs differentiate into club cells and ciliated cells to regenerate bronchiolar epithelium or generate AT1 and AT2 alveolar cells to partially restore alveoli, respectively (Fig. 7).

Clearly, BASCs do not contribute to all new airway cells after bronchiolar injury or to all new AT1 or AT2 cells after alveolar injury. Many other resident stem cells such as club cells or resident AT2 cells[5,13–15] are also responsible for repair and regeneration of lung epithelial cells. In the face of injury, lung-resident stem cells are activated and subsequently proliferate and differentiate into different lineages to effectively repair and regenerate the injured lung[44].
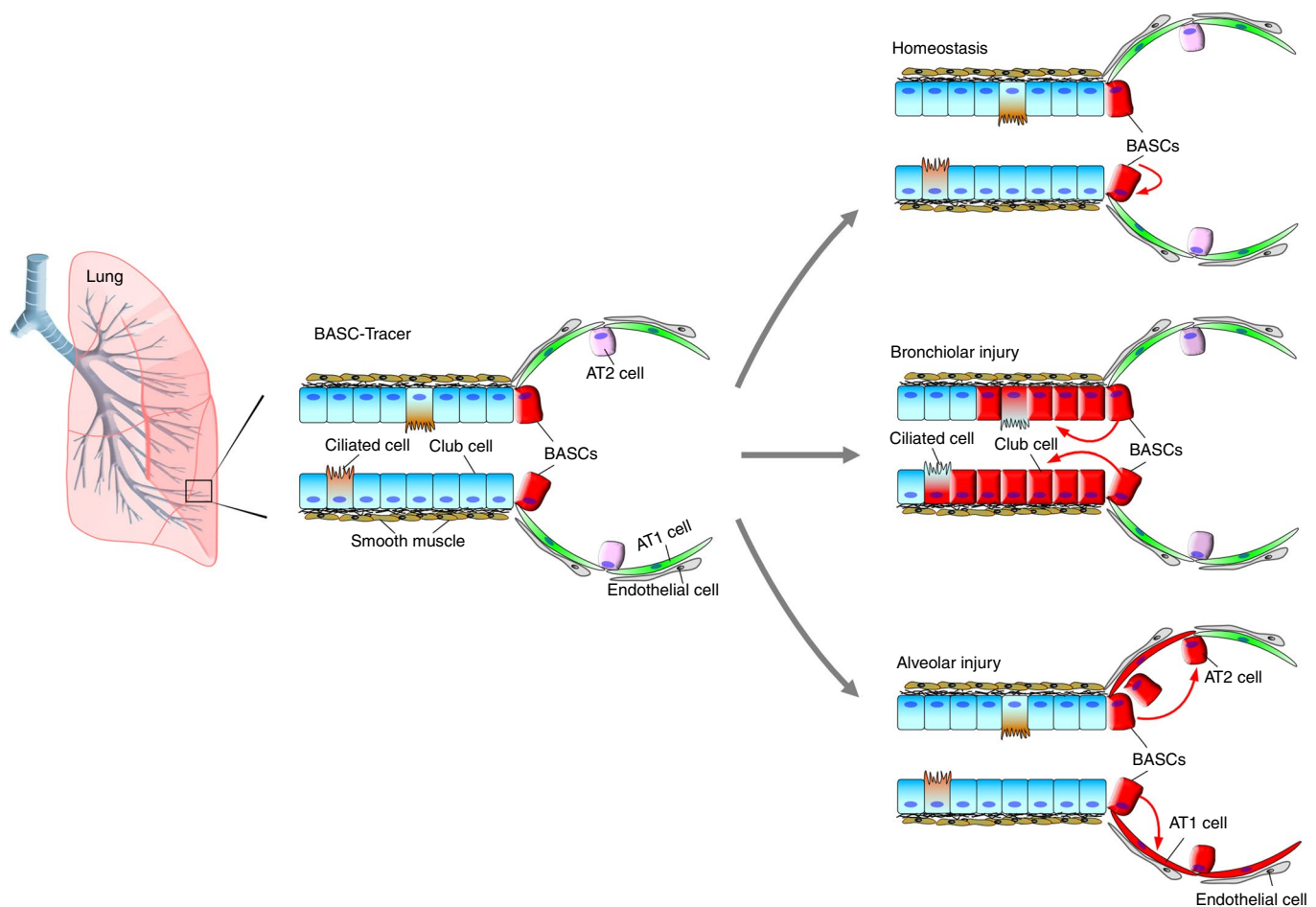
Fig. 7 | BASCs are multipotent resident epithelial stem cells for lung repair and regeneration. Cartoon image showing labeling of BASCs by using BASC-Tracer mice (left). These labeled BASCs (red) undergo slow self-renewal during lung homeostasis (top right); respond to bronchiolar injury and generate new club cells and ciliated cells in terminal bronchioles (middle right); and expand substantially in alveolar injury and differentiate into AT1 and AT2 cells (bottom right).

In the large airways, basal stem cells give rise to differentiated club cells and ciliated cells[12], and continuously serve as niches for their daughter secretory cells[45]. Their descendant club cells in the bronchioles self-renew and differentiate into ciliated cells[13], and these differentiated club cells can also revert into functional stem cells after basal-cell depletion[19]. In the bronchiolar injuries, club cells mainly repair airway epithelial cells[13,14]. In the alveoli, AT2 cells generate both AT1 and AT2 cells under homeostatic conditions as well as upon damage[5,15]. In contrast, a subset of AT1 cells expressing Hopx can replicate and generate type 2 stem cells after partial pneumonectomy[46]. These studies support a model in which dedicated stem or progenitor cells are responsible for repair of bronchioles and alveoli; for example, club cells are responsible for repairing bronchioles, and AT2 cells generate AT1 cells after alveolar injuries[2,15–17]. Our work showed that, beyond these known lung stem cells, BASCs respond and react distinctly to different injuries through differentiation into multiple cell lineages such as club cells, ciliated cells, AT1 and AT2 cells (Fig. 7). Because deployment of lung stem cells for tissue repair and regeneration is also dependent on the type and severity of injuries[8,18,19,47]. The populations of stem cells activated under different injury conditions and the factors that determine the activated population are important questions that merit further investigation. The BASC transcriptome is an intermediate between that of club cells and AT2 cells, and it also contains several uniquely expressed genes. Because BASCs share some gene expression signatures with club and AT2 cells, they may also have the potential to differentiate into both bronchiolar and alveolar cell lineages. BASCs have also been reported to exist in established lung tumors[21], thus indicating their contribution to lung-tumor formation. Whether these endogenous BASCs are the putative tumor stem-cell population for subtypes of lung cancer remains to be determined in the future. Additionally, understanding the transcriptional regulation underpinning the multipotency of BASCs and the role of crucial niches at BADJ regions may also provide new insights into lung repair and regeneration.

URLs. ImageJ software, http://rsb.info.nih.gov/ij/; Hisat2, https://ccb.jhu.edu/software/hisat2/index.shtml; Htseq-count, https://htseq.readthedocs.io; Seurat, https://cran.r-project.org/web/packages/Seurat/index.html; DESeq2, http://bioconductor.org/packages/devel/bioc/vignettes/DESeq2/inst/doc/DESeq2.html; GEO database, https://www.ncbi.nlm.nih.gov/geo/.

Online content
Any methods, additional references, Nature Research reporting summaries, source data, statements of data availability and associated accession codes are available at https://doi.org/10.1038/s41588-019-0346-6.

References
1. Kuo, C. S. & Krasnow, M. A. Formation of a neurosensory organ by epithelial cell slithering. *Cell* **163**, 394–405 (2015).

2. Morrisey, E. E. & Hogan, B. L. Preparing for the first breath: genetic and cellular mechanisms in lung development. *Dev. Cell* **18**, 8–23 (2010).

3. Rock, J. R. & Hogan, B. L. Epithelial progenitor cells in lung development, maintenance, repair, and disease. *Annu. Rev. Cell Dev. Biol.* **27**, 493–512 (2011).

4. Hogan, B. L. et al. Repair and regeneration of the respiratory system: complexity, plasticity, and mechanisms of lung stem cell function. *Cell Stem Cell* **15**, 123–138 (2014).

5. Desai, T. J., Brownfield, D. G. & Krasnow, M. A. Alveolar progenitor and stem cells in lung development, renewal and cancer. *Nature* **507**, 190–194 (2014).

6. Kumar, P. A. et al. Distal airway stem cells yield alveoli in vitro and during lung regeneration following H1N1 influenza infection. *Cell* **147**, 525–538 (2011).

7. Chen, F. & Krasnow, M. A. Progenitor outgrowth from the niche in *Drosophila* trachea is guided by FGF from decaying branches. *Science* **343**, 186–189 (2014).

8. Zuo, W. et al. p63+Krt5+ distal airway stem cells are essential for lung regeneration. *Nature* **517**, 616–620 (2014).

9. Peng, T. et al. Hedgehog actively maintains adult lung quiescence and regulates repair and regeneration. *Nature* **526**, 578–582 (2015).

10. Hong, K. U., Reynolds, S. D., Watkins, S., Fuchs, E. & Stripp, B. R. Basal cells are a multipotent progenitor capable of renewing the bronchial epithelium. *Am. J. Pathol.* **164**, 577–588 (2004).

11. Hong, K. U., Reynolds, S. D., Watkins, S., Fuchs, E. & Stripp, B. R. In vivo differentiation potential of tracheal basal cells: evidence for multipotent and unipotent subpopulations. *Am. J. Physiol. Lung Cell. Mol. Physiol.* **286**, L643–L649 (2004).

12. Rock, J. R. et al. Basal cells as stem cells of the mouse trachea and human airway epithelium. *Proc. Natl Acad. Sci. USA* **106**, 12771–12775 (2009).

13. Rawlins, E. L. et al. The role of Scgb1a1+ Clara cells in the long-term maintenance and repair of lung airway, but not alveolar, epithelium. *Cell Stem Cell* **4**, 525–534 (2009).

14. Hong, K. U., Reynolds, S. D., Giangreco, A., Hurley, C. M. & Stripp, B. R. Clara cell secretory protein-expressing cells of the airway neuroepithelial body microenvironment include a label-retaining subset and are critical for epithelial renewal after progenitor cell depletion. *Am. J. Respir. Cell Mol. Biol.* **24**, 671–681 (2001).

15. Barkauskas, C. E. et al. Type 2 alveolar cells are stem cells in adult lung. *J. Clin. Invest.* **123**, 3025–3036 (2013).

16. Zacharias, W. J. et al. Regeneration of the lung alveolus by an evolutionarily conserved epithelial progenitor. *Nature* **555**, 251–255 (2018).

17. Nabhan, A., Brownfield, D. G., Harbury, P. B., Krasnow, M. A. & Desai, T. J. Single-cell Wnt signaling niches maintain stemness of alveolar type 2 cells. *Science* **359**, 1118–1123 (2018).

18. Vaughan, A. E. et al. Lineage-negative progenitors mobilize to regenerate lung epithelium after major injury. *Nature* **517**, 621–625 (2014).

19. Tata, P. R. et al. Dedifferentiation of committed epithelial cells into stem cells in vivo. *Nature* **503**, 218–223 (2013).

20. Giangreco, A., Reynolds, S. D. & Stripp, B. R. Terminal bronchioles harbor a unique airway stem cell population that localizes to the bronchoalveolar duct junction. *Am. J. Pathol.* **161**, 173–182 (2002).

21. Kim, C. F. et al. Identification of bronchioalveolar stem cells in normal lung and lung cancer. *Cell* **121**, 823–835 (2005).

22. Nolen-Walston, R. D. et al. Cellular kinetics and modeling of bronchioalveolar stem cell response during lung regeneration. *Am. J. Physiol. Lung Cell. Mol. Physiol.* **294**, L1158–L1165 (2008).

23. Dovey, J. S., Zacharek, S. J., Kim, C. F. & Lees, J. A. Bmi1 is critical for lung tumorigenesis and bronchioalveolar stem cell expansion. *Proc. Natl Acad. Sci. USA* **105**, 11857–11862 (2008).

24. Zacharek, S. J. et al. Lung stem cell self-renewal relies on BMI1-dependent control of expression at imprinted loci. *Cell Stem Cell* **9**, 272–281 (2011).

25. Lee, J. H. et al. Lung stem cell differentiation in mice directed by endothelial cells via a bmp4-nfatc1-thrombospondin-1 axis. *Cell* **156**, 440–455 (2014).

26. He, L. et al. Enhancing the precision of genetic lineage tracing using dual recombinases. *Nat. Med.* **23**, 1488–1498 (2017).

27. Zhang, H. et al. Genetic lineage tracing identifies endocardial origin of liver vasculature. *Nat. Genet.* **48**, 537–540 (2016).

28. Madisen, L. et al. Transgenic mice for intersectional targeting of neural sensors and effectors with high specificity and performance. *Neuron* **85**, 942–958 (2015).

29. Madisen, L. et al. A robust and high-throughput cre reporting and characterization system for the whole mouse brain. *Nat. Neurosci.* **13**, 133–140 (2010).

30. Zhang, H. et al. Endocardium contributes to cardiac fat. *Circ. Res.* **118**, 254–265 (2016).

31. Reinert, R. B. et al. Tamoxifen-induced Cre-loxP recombination is prolonged in pancreatic islets of adult mice. *PLoS One* **7**, e33529 (2012).

32. Rock, J. R. et al. Multiple stromal populations contribute to pulmonary fibrosis without evidence for epithelial to mesenchymal transition. *Proc. Natl Acad. Sci. USA* **108**, E1475–E1483 (2011).

33. Snippert, H. J. et al. Intestinal crypt homeostasis results from neutral competition between symmetrically dividing Lgr5 stem cells. *Cell* **143**, 134–144 (2010).

34. Montoro, D. T. et al. A revised airway epithelial hierarchy includes CFTR-expressing ionocytes. *Nature* **12771**, 319–324 (2018).

35. Plasschaert, L. W. et al. A single-cell atlas of the airway epithelium reveals the CFTR-rich pulmonary ionocyte. *Nature* **545**, 377–381 (2018).

36. Honda, H. et al. Leucine-rich α-2 glycoprotein promotes lung fibrosis by modulating TGF-β signaling in fibroblasts. *Physiol. Rep.* **5**, e13556 (2017).

37. Wang, X. et al. LRG1 promotes angiogenesis by modulating endothelial TGFβ signalling. *Nature* **499**, 306–311 (2013).

38. Schultz, C. J., Torres, E., Londos, C. & Torday, J. S. Role of adipocyte differentiation-related protein in surfactant phospholipid synthesis by type II cells. *Am. J. Physiol. Lung Cell. Mol. Physiol.* **283**, L288–L296 (2002).

39. El Agha, E. et al. Two-way conversion between lipogenic and myogenic fibroblastic phenotypes marks the progression and resolution of lung fibrosis. *Cell Stem Cell* **20**, 261–273.e3 (2016).

40. Zhang, X. et al. Comparative membrane proteomic analysis between lung adenocarcinoma and normal tissue by iTRAQ labeling mass spectrometry. *Am. J. Transl. Res.* **6**, 267–280 (2014).

41. Zhang, X. D. et al. Identification of adipophilin as a potential diagnostic tumor marker for lung adenocarcinoma. *Int. J. Clin. Exp. Med.* **7**, 1190–1196 (2014).

42. Xu, X. et al. Evidence for type II cells as cells of origin of K-Ras-induced distal lung adenocarcinoma. *Proc. Natl Acad. Sci. USA* **109**, 4910–4915 (2012).

43. Noh, M. S. et al. Magnetic surface-enhanced Raman spectroscopic (M-SERS) dots for the identification of bronchioalveolar stem cells in normal and lung cancer mice. *Biomaterials* **30**, 3915–3925 (2009).

44. Kotton, D. N. & Morrisey, E. E. Lung regeneration: mechanisms, applications and emerging stem cell populations. *Nat. Med.* **20**, 822–832 (2014).

45. Pardo-Saganta, A. et al. Parent stem cells can serve as niches for their daughter cells. *Nature* **523**, 597–601 (2015).

46. Jain, R. et al. Plasticity of Hopx+ type I alveolar cells to regenerate type II cells in the lung. *Nat. Commun.* **6**, 6727 (2015).

47. Giangreco, A. et al. Stem cells are dispensable for lung homeostasis but restore airways after injury. *Proc. Natl Acad. Sci. USA* **106**, 9286–9291 (2009).

Author contributions

Q.L., K.L. and B.Z. designed the study and wrote the manuscript. Q.L., K.L. and G.C. performed experiments and analyzed the data. W.G., G.C., G.P. and N.J. performed scRNA-seq and analyzed data. X.H., S.Y., Z.Q., Y.L., R.Y., W.P., L.Z., L.H., H.Z., W.Y., M.T., X.T., D.C., Y.N., S.H., T.R., Z.Q., H.H. and Y.A.Z. bred the mice, performed experiments or provided material, important suggestions and valuable comments. H.J. designed the study and provided valuable comments. B.Z. supervised the study and analyzed the data.

Competing interests

The authors declare no competing interests.

Additional information

Methods

Mice. All mice were used in accordance with the guidelines of the Institutional Animal Care and Use Committee of the Institute for Nutritional Sciences and Shanghai Institute of Biochemistry and Cell Biology, Shanghai Institute for Biological Sciences, Chinese Academy of Sciences. The *Sftpc–DreER* mouse line was generated by the Nanjing Biomedical Research Institute of Nanjing University. The *Sftpc–DreER* knock-in mouse line was generated by insertion of a cDNA encoding Dre recombinase fused with a mutant form of the estrogen-receptor hormone-binding domain in frame with the translational start codon (ATG) of the *Sftpc* gene, as previously described[48]. In brief, a 129 mouse BAC clone containing the complete mouse *Sftpc* gene was obtained from the Sanger Institute. A targeting vector was constructed containing the following cassettes: DreER cDNA, SV40 poly(A) sequence and Frt site-flanked PGK-EM7-Neo resistance gene. Two homologous arms on both sides of the ATG of the *Sftpc* gene were generated in targeting vectors by recombination from BAC. Then the linearized targeting vector was electroporated into mouse embryonic stem cells (ESCs). The targeting vector containing the aforementioned cassettes was knocked into the *Sftpc* locus for endogenous expression of DreER. After G418 selection, approximately 200 clones were chosen for genomic-DNA purification and examination of positive clones. We screened neomycin-resistant clones for correct gene targeting by PCR assays with primer pairs spanning the targeting vector and flanking genomic DNA. After confirmation of correct targeting and karyotype, positive ESC clones were expanded and injected into blastocysts for the generation of mice. The obtained chimeric mouse lines were crossed to 129 lines for germline transmission. PCR primers spanning the genomic DNA and inserted DNA sequence were designed to test the correct targeted allele. Genotyping sequences are available upon request. The established *Sftpc–DreER* mouse line was maintained on a C57B6/129 mixed background. *Scgb1a1–CreER*, *R26–tdTomato*, *Rosa26–RSR–tdTomato* and *Rosa26–RSR–LSL–tdTomato*[4] mice have been described previously[13,28–30]. All mice were maintained on the C57BL6/129 mixed background and kept under a 12-h day and light cycle. To lineage label BASCs, we gavaged BASC-Tracer (*Scgb1a1–CreER;Sftpc–DreER;R26–RSR–LSL–tdTomato* triple-knock-in mice) with 25 μg g⁻¹ tamoxifen (Sigma, T5648, 2.5 mg ml⁻¹ dissolved in corn oil) at the indicated times. To characterize the cell types labeled by *Scgb1a1–CreER* or *Sftpc–DreER* individually, we gavaged *Scgb1a1–CreER;R26–tdTomato* or *Sftpc–DreER;R26–RSR–tdTomato* mice with 0.2 mg g⁻¹ tamoxifen (Sigma, T5648, 20 mg ml⁻¹ dissolved in corn oil). To test the orthogonal recombination by Cre or Dre recombinase, we generated *Scgb1a1–CreER;R26–RSR–LSL–tdTomato* or *Sftpc–DreER;R26–RSR–LSL–tdTomato* mice. These mice were gavaged with 25 μg g⁻¹ tamoxifen. Mice were randomly assigned to different experimental groups, and the investigators were not blinded to mice allocation during experiments and analysis.

Genomic PCR. Genomic DNA was prepared from transgenic mouse tails. Tissues were lysed by incubation with lysis buffer (100 mM Tris HCl, pH 7.8, 5 mM EDTA, 0.2% SDS, 200 mM NaCl and 100 μg ml⁻¹ proteinase K) overnight at 55 °C, and this was followed by centrifugation at maximum speed for 5 min to obtain supernatant with genomic DNA. DNA was precipitated with isopropanol, washed in 70% ethanol and dissolved in deionized water. All mice were genotyped with genomic PCR as described previously[49].

Naphthalene injury and EdU incorporation. Bronchiolar-injury models were conducted by using naphthalene intraperitoneal injection, as previously described[20]. Naphthalene (Sigma 84679) was freshly dissolved in sterile corn oil at a concentration of 25 mg ml⁻¹. To trace the fate of BASCs in the bronchiolar-injury model, we gavaged BASC-Tracer mice with 25 μg g⁻¹ tamoxifen at 7 weeks of age, and then injected them intraperitoneally with 250 mg kg⁻¹ naphthalene 1 or 3 weeks after tamoxifen induction. Mouse lungs were collected 5–7 weeks after injury. Vehicle-control mice were treated with tamoxifen (25 μg g⁻¹) at the same time and intraperitoneally injected with 10 μl g⁻¹ sterile corn oil. For EdU incorporation experiments, 10 μg g⁻¹ EdU was intraperitoneally injected into mice 48 h after naphthalene or vehicle treatment. Tissues were collected 6–8 h after EdU injection. To quantify tdTomato⁺ club-cell height in each BADJ, we designated the most distal tdTomato⁺CC10⁺ cells lining the terminal bronchioles as the number 1 club cell.

Bleomycin injury and EdU incorporation. Alveolar injury was achieved by intratracheal instillation of bleomycin[32,50]. Bleomycin (Sigma B8416) was dissolved in sterile PBS (Invitrogen, 10010049) at a concentration of 10 U ml⁻¹, stored as small aliquots at −80 °C, and diluted 1:10 to 1 U ml⁻¹ with PBS before use. Mice were anesthetized by intraperitoneal injection with 1% pentobarbital sodium (8 μl pentobarbital per g body weight). When a mouse did not respond to stimuli, it was suspended on its back on an ~60° inclined board with a band running under its upper incisors. The mouth was then opened with padded forceps, and the mouse was intratracheally intubated with a 22-G tip-removed cannula needle. Then 2 U kg⁻¹ (2 μl g⁻¹ at a concentration of 1 U ml⁻¹) bleomycin was pipetted into the cannula. Along with the mouse breath, bleomycin was inhaled into the lung. Vehicle-control-group mice were anesthetized and intratracheally instilled with 2 μl g⁻¹ sterile PBS (Invitrogen, 10010049). Lung tissues were collected approximately 2 months after injury for sectioning and staining. For EdU-incorporation experiments, mice were

intraperitoneally injected with 10 μg g⁻¹ EdU 2.5 weeks after bleomycin or vehicle instillation, and lungs were collected 24 h later.

Lung tissue collection and whole-mount microscopy. Mice were killed by cervical dislocation, and then the blood in the lungs was flushed out by perfusion with 10–15 ml cold PBS through the right ventricle. Collected mouse lungs were then washed with PBS and placed on agar to obtain whole-mount bright-field and fluorescence images by using a Zeiss stereoscope (AxioZoom V16). To determine the magnification of specific regions, we used the automated z-stack images acquired with a Zeiss stereoscope (AxioZoom V16).

Immunostaining of lung sections. Lungs were first fixed for approximately 15 min by perfusion with ~1 ml cold 4% PFA through the trachea and then dissected from mice and subjected to continued fixing in PFA for 1 h at 4 °C. After being washed three times in 30% PBS, lungs were dehydrated in 30% sucrose overnight and embedded in OCT (Sakura). Cryosections (~10 μm) were collected on negatively charged slides and stored at −20 °C until use. The dried sections were washed twice with PBS and then blocked with 5% normal donkey serum in PBST (0.2% Triton X-100 in PBS). Sections were stained with primary antibodies at 4 °C overnight and then washed with PBS three times and incubated with Alexa-conjugated secondary antibodies (Invitrogen or Jackson ImmunoResearch) for 30 minutes at room temperature. Sections were then washed with PBS three times and mounted with mounting medium containing DAPI (Vector Labs). For weak signals, we used horseradish peroxidase– or biotin-conjugated secondary antibodies, and detected the signal by using a tyramide signal amplification kit (PerkinElmer)[51] or fluorescently conjugated streptavidin. Primary antibodies to the following were used: SPC (Millipore, AB3786, 1:200), PDPN or T1a (DSHB, 8.1.1, 1:200), CC10 (Santa Cruz, SC-9772, 1:200), tdTomato (Rockland 600-401-379, 1:1,000), tdTomato (ChromoTek, abin334653, 1:200), Keratin5 (Covance, PRB-160p, 1:200), VE-cadherin (R&D, AF1002, 1:200), PEGFRa (R&D AF1062, 1:500), PDGFRb (eBioscience, 14-1402, 1:500), PECAM (BD Pharmmingen, 553370, 1:500), aSMA (Sigma, F3777, 1:200), CGRP (Sigma, C8198, 1:500), β-tubulin (Abcam, ab6046, 1:200), β-tubulin (BioGenex, Mu178-5UC, 1:500), p63 (Biolegend, 619001, 1:100) and acetylated tubulin (Sigma, T7451, 1:500). The secondary antibodies were Alexa donkey anti-rabbit 488 (Invitrogen, A21206, 1:1,000), Alexa donkey anti-rabbit 555 (Invitrogen, A31572, 1:1,000), Dylight 549 donkey anti-rat IgG(H + L) (JIR, 712-505-153, 1:1,000), Alexa donkey anti-goat 488 (Invitrogen, A11055, 1:1,000), Alexa goat anti-hamster IgG(H + L) 488 (Invitrogen, A21110, 1:1,000), Biotin-sp-a-rabbit IgG (JIR, 711-065-152, 1:1,000), Dylight 647-streptavidin (JIR, 016-490-084, 1:1,000), Alexa donkey anti-goat 647 (Invitrogen, A21447, 1:1,000), Alexa donkey anti-rat 488 (Invitrogen, A21808, 1:1,000) immpress-rat immunoglobulin (goat) (Vector, MP-7444-15), Alexa donkey anti-mouse 488 (Invitrogen, A21202, 1:1,000), immpress-rabbit immunoglobulin (horse) (Vector, MP-7401) and Fluorescein Amplification Reagent (PerkinElmer, NEL741001KT). Pictures were taken with an Olympus FV1200 or Zeiss LSM 800 confocal system.

Lung-cell isolation and FACS sorting. Lung cells were isolated as previously reported[32]. In brief, mice were killed by cervical dislocation and perfused with 10 ml cold PBS through the right ventricle to flush out blood cells in the lung. Then the mice were inflated through the trachea with 2 ml PBS and 1.5 ml protease solution (collagenase type I (500 U ml⁻¹; Gibco 17100–017), elastase (4 U ml⁻¹; Worthington Biochemical Corporation LS002279), dispase (5 U ml⁻¹; BD Biosciences 354235) and DNase I (0.33 U ml⁻¹; Worthington Biochemical Corporation LS002139) in DMEM/F12 (Gibco, 10565018)) sequentially. The lungs were cut into small pieces and incubated in 2.5 ml protease solution for 25 min at 37 °C with frequent agitation. After vigorous shaking, the tissue was disrupted by pipetting, centrifuged at 1,000g for 5 min, washed with DMEM/F12 and recentrifuged. The pellet was suspended in 2 ml 0.1% Trypsin-EDTA with DNase I and incubated for 20 minutes at 37 °C with intermittent agitation. An equal volume of DMEM/F12 with 10% FBS (Gibco, 10099141) was added to block trypsin, and cells were filtered through a 100-μm strainer, centrifuged and incubated in red-blood-cell lysis buffer (2–5 ml, eBioscience, 00-4333-57) at room temperature for 5 min. An equal volume of PBS was added, and cells were filtered through a 40-μm strainer, centrifuged and resuspended in PBS. The cells were then stained for flow cytometry analysis and sorting[52]. The cells were stained with a LIVE/DEAD Fixable Violet Dead Cell Stain Kit (Life Technologies, L34955) at 4 °C for 25 min according to the manufacturer's instructions. After addition of 500 μl isolation buffer (2 mM EDTA and 0.5% BSA in PBS), the cells were centrifuged at 4,600g for 1–2 min, and the pellet was blocked in Fc block (eBioscience, 14-0161, 1:100) for 5 min and stained in antibody mixture containing anti-CD45 PE-Cy7 (eBioscience, 25-0451, 1:400), anti-CD31 PE-Cy7 (eBioscience, 25-0311, 1:40) or anti-CD326 APC (eBioscience, 17-5791, 1:100). After staining for 30 minutes at 4 °C, the cells were washed with isolation buffer, and live tdTomato⁺ epithelial cells were sorted with a CD45⁻CD31⁻CD326⁺tdTomato⁺ gating strategy on a BD FACSAria II flow cytometer.

Single-cell clonal analysis of BASCs. To trace single CC10⁺SPC⁺ BASCs, we generated a confetti reporter line that responded to both Dre and Cre recombinases, *R26–Confetti2*, in which CAG–rox–Stop–rox–Confetti was targeted to the Rosa26 gene locus. The *Sftpc–DreER;Scgb1a1–CreER;R26–Confetti2* mouse

line was generated to perform clonal analysis of single BASCs. For tracing the fate of sparsely labeled single BASCs in the bronchiolar or alveolar-injury models, we treated *Sftpc–DreER;Scgb1a1–CreER;R26–Confetti2* mice with tamoxifen at 7 weeks of age, and then subjected them to naphthalene or bleomycin treatment for bronchiolar or alveolar injury, respectively, as described above. Mouse lungs were collected 5–7 weeks after naphthalene injury or 8–10 weeks after bleomycin injury. Images were taken with an Olympus confocal microscopy system (FV1200), and fluorescence signals were analyzed with ImageJ (NIH) software. For clonal analysis of the naphthalene- or vehicle-treatment groups, the single string fluorescence$^+$CC10$^+$club cell number or single fluorescence$^+$SPC$^+$ AT2-cell number was quantified for each BADJ field. For clonal analysis in bleomycin- or vehicle-treatment groups, the single fluorescence$^+$CC10$^+$, single fluorescence$^+$SPC$^+$ or single fluorescence$^+$T1a$^+$ cell number was quantified for each BADJ field.

scRNA-seq. tdTomato$^+$ epithelial cells were sorted from BASC-Tracer, *Scgb1a1– CreER; Rosa26–LSL–tdTomato* and *Sftpc–DreER; Rosa26–RSR–tdTomato* mice 1 week after tamoxifen induction, by using the CD45$^-$CD31$^-$CD326$^+$tdTomato$^+$ gating strategy. Single cells were sorted into 96-well plates (Bio-Rad, HSP9601) on ice and subjected to a modified full-length single-cell RNA-seq protocol (Smart-seq2)[53,54]. In brief, cells were lysed in single-cell RNA lysis buffer containing 0.45% (vol/vol) NP-40, then subjected to reverse transcription with SuperScript II reverse transcriptase (Invitrogen) and whole transcription amplification with KAPA HiFi HotStart ReadyMix (2×; KAPA Biosystems). PCR products were purified with AMPure XP beads (Agencourt) and quantified with a Qubit dsDNA HS Assay Kit (Thermo Fisher). cDNA libraries were constructed with a Nextera XT DNA Library Preparation Kit (Illumina) and sequenced on an Illumina HiSeq X Ten instrument in 150-bp paired-end-read mode by BerryGenomics. In total, 480 single cells were sequenced for analysis. The amplification, cDNA purification and library construction were done on the Agilent Bravo automatic liquid-handling platform in the core facility for molecular biology at SIBCB.

scRNA-seq data analysis. The sequencing quality of all raw sequencing data was evaluated by FASTQC. Reads were mapped to the mouse GRCm38 genome assemblies by HISAT2 (ref. [55]) with default settings. Uniquely aligned reads were counted by using the 'htseq-count' tool in HTSeq[56]. $\log_2$(TPM + 1) expression values were computed by using the Rcpp-based function in the R package 'Seurat'. Highly variable genes were used for principal-component analysis in Seurat. After principal-component analysis, significant principal components were identified by using the knee in the scree plot, which identified ten significant principal components. Only scores from these significant principal components were used as the input to nearest-neighbor based clustering ('FindClusters') and *t*-SNE ('RunTSNE', perplexity $P = 30$), both of which were from the 'Seurat' package[57].

Signature cluster genes were identified by using DESeq2 (ref. [58]) with $\log_2$ (fold change) >1.5 and at a false discovery rate <0.01.

Statistics. Data are presented as means ± s.d., and the data are shown in box-and-whiskers plots with minimum to maximum ranges. Statistical analysis was performed by using two-tailed unpaired Student's *t* tests for comparison of differences between two groups. $P < 0.05$ was considered to be statistically significant.

Reporting Summary. Further information on research design is available in the Nature Research Reporting Summary linked to this article.

Data availability
The generated sequencing data have been deposited in the GEO database under accession code GSE118891.

References
48. Tian, X. et al. Subepicardial endothelial cells invade the embryonic ventricle wall to form coronary arteries. *Cell Res.* **23**, 1075–1090 (2013).
49. Liu, Q. et al. Genetic targeting of sprouting angiogenesis using Apln-CreER. *Nat. Commun.* **6**, 6020 (2015).
50. Degryse, A. L. et al. Repetitive intratracheal bleomycin models several features of idiopathic pulmonary fibrosis. *Am. J. Physiol. Lung Cell. Mol. Physiol.* **299**, L442–L452 (2010).
51. He, L. et al. Preexisting endothelial cells mediate cardiac neovascularization after injury. *J. Clin. Invest.* **127**, 2968–2981 (2017).
52. Liu, Q. et al. Genetic lineage tracing identifies in situ Kit-expressing cardiomyocytes. *Cell Res.* **26**, 119–130 (2016).
53. Chen, J. et al. Spatial transcriptomic analysis of cryosectioned tissue samples with Geo-seq. *Nat. Protoc.* **12**, 566–580 (2017).
54. Picelli, S. et al. Smart-seq2 for sensitive full-length transcriptome profiling in single cells. *Nat. Methods* **10**, 1096–1098 (2013).
55. Pertea, M., Kim, D., Pertea, G. M., Leek, J. T. & Salzberg, S. L. Transcript-level expression analysis of RNA-seq experiments with HISAT, StringTie and Ballgown. *Nat. Protoc.* **11**, 1650–1667 (2016).
56. Anders, S., Pyl, P. T. & Huber, W. HTSeq: a Python framework to work with high-throughput sequencing data. *Bioinformatics* **31**, 166–169 (2015).
57. Kiselev, V. Y. et al. SC3: consensus clustering of single-cell RNA-seq data. *Nat. Methods* **14**, 483–486 (2017).
58. Love, M. I., Huber, W. & Anders, S. Moderated estimation of fold change and dispersion for RNA-seq data with DESeq2. *Genome Biol.* **15**, 550 (2014).

nature research

Corresponding author(s):   Bin Zhou, Hongbin Ji, Guangdun Peng

Life Sciences Reporting Summary

Nature Research wishes to improve the reproducibility of the work that we publish. This form is intended for publication with all accepted life science papers and provides structure for consistency and transparency in reporting. Every life science submission will use this form; some list items might not apply to an individual manuscript, but all fields must be completed for clarity.

For further information on the points included in this form, see Reporting Life Sciences Research. For further information on Nature Research policies, including our data availability policy, see Authors & Referees and the Editorial Policy Checklist.

Please do not complete any field with "not applicable" or n/a. Refer to the help text for what text to use if an item is not relevant to your study.
For final submission: please carefully check your responses for accuracy; you will not be able to make changes later.

▶ Experimental design

1. **Sample size**

   Describe how sample size was determined.

   For all the experiments, 4-6 mouse samples were used in each experiments according to standard scientific conventions, and detailed sample size was indicated in each figure legend. No statistical methods were used to predetermine the sample size.

2. **Data exclusions**

   Describe any data exclusions.

   No data were excluded from the analysis

3. **Replication**

   Describe the measures taken to verify the reproducibility of the experimental findings.

   For each experiment all replication attempts were successful. For all the data showing in the work, at least 4 repeats were performed to verify the reproducibility of the experimental findings.

4. **Randomization**

   Describe how samples/organisms/participants were allocated into experimental groups.

   Both female and male mice at the same age were used in our study and randomly allocated into different treatment groups.

5. **Blinding**

   Describe whether the investigators were blinded to group allocation during data collection and/or analysis.

   The investigators were not blind to group allocation during data collection and analysis. For the injury models, we use the same genotype mice and assign them into control (vehicle) and injury experiment groups randomly and blinded. For analysis, because there is a significant difference between control and injuried lungs, the investigators are not blinded to the control and injury groups.

   Note: all in vivo studies must report how sample size was determined and whether blinding and randomization were used.

6. Statistical parameters

For all figures and tables that use statistical methods, confirm that the following items are present in relevant figure legends (or in the Methods section if additional space is needed).

n/a	Confirmed
☐	☒ The <u>exact sample size</u> (*n*) for each experimental group/condition, given as a discrete number and unit of measurement (animals, litters, cultures, etc.)
☐	☒ A description of how samples were collected, noting whether measurements were taken from distinct samples or whether the same sample was measured repeatedly
☐	☒ A statement indicating how many times each experiment was replicated
☐	☒ The statistical test(s) used and whether they are one- or two-sided *Only common tests should be described solely by name; describe more complex techniques in the Methods section.*
☐	☒ A description of any assumptions or corrections, such as an adjustment for multiple comparisons
☐	☒ Test values indicating whether an effect is present *Provide confidence intervals or give results of significance tests (e.g. P values) as exact values whenever appropriate and with effect sizes noted.*
☐	☒ A clear description of statistics including <u>central tendency</u> (e.g. median, mean) and <u>variation</u> (e.g. standard deviation, interquartile range)
☐	☒ Clearly defined error bars in <u>all</u> relevant figure captions (with explicit mention of central tendency and variation)

See the web collection on statistics for biologists for further resources and guidance.

▶ Software

Policy information about availability of computer code

7. Software

Describe the software used to analyze the data in this study.

> Image J (FIJI) and Photoline 20.02 were used for immunofluorescence and histology images analysis, Graph pad prism 6.0 was use for data analysis. HTSAT2, HTSeq, R, DESeq, Seurat were used for scRNA-seq analysis.

For manuscripts utilizing custom algorithms or software that are central to the paper but not yet described in the published literature, software must be made available to editors and reviewers upon request. We strongly encourage code deposition in a community repository (e.g. GitHub). *Nature Methods* guidance for providing algorithms and software for publication provides further information on this topic.

▶ Materials and reagents

Policy information about availability of materials

8. Materials availability

Indicate whether there are restrictions on availability of unique materials or if these materials are only available for distribution by a third party.

> All materials are readily available from the authors or from commercial resources

9. Antibodies

Describe the antibodies used and how they were validated for use in the system under study (i.e. assay and species).

> The followings are all the antibodies we used in this study:SPC (Millipore, AB3786, 1:200), PDPN or T1a (DSHB, 8.1.1, 1:200), CC10 (Santa Cruz, SC-9772, 1:200), tdTomato (Rockland 600-401-379, 1:1000), tdTomato (ChromoTek, abin334653, 1:200), Keratin5 (Covance, PRB-160p, 1:200), VE-cadherin (R&D, AF1002, 1:200), PEGFRa (R&D AF1062, 1:500), PDGFRb (eBioscience, 14-1402, 1:500), PECAM (BD pharmmingen, 553370, 1:500), aSMA (Sigma, F3777, 1:200), CGRP (Sigma, C8198, 1:500), beta-tubulin (Abcam, ab6046, 1:200),beta-tubulin (BioGenex, Mu178-5UC, 1:500), P63 (Biolegend, 619001, 1:100), Acetylated tubulin (Sigma, T7451, 1:500), CD45 PE-Cy7 (eBioscience, 25-0451, 1:400), CD31 PE-Cy7 (eBioscience, 25-0311, 1:40) and CD326 APC (eBioscience, 17-5791, 1:100). Alexa donkey anti rabbit 488 (Invitrogen, A21206, 1:1000), Alexa donkey a-rabbit 555 (Invitrogen, A31572, 1:1000), Dylight 549 donkey anti-rat IgG(H+L) (JIR, 712-505-153, 1:1000), Alexa donkey a-goat 488 (Invitrogen, A11055, 1:1000), Alexa goat anti hamster IgG(H+L) 488 (Invitrogen, A21110, 1:1000), Biotin-sp-a-rabbit IgG (JIR, 711-065-152, 1:1000), Dylight 647-Streptavidin (JIR, 016-490-084, 1:1000), Alexa donkey anti-goat 647 (Invitrogen, A21447, 1:1000),Alexa donkey anti-rat 488 (Invitrogen, A21808, 1:1000) immpress-rat Ig (goat) (Vector, MP-7444-15), Alexa donkey a-mouse 488 (Invitrogen, A21202, 1:1000), immpress-rabbit Ig (horse) (Vector, MP-7401), Fluorescein Amplification Reagent (PerkinElmer, NEL741001KT)

10. Eukaryotic cell lines

    a. State the source of each eukaryotic cell line used.

        We did not use any cell line.

    b. Describe the method of cell line authentication used.

        We did not use any cell line.

    c. Report whether the cell lines were tested for mycoplasma contamination.

        We did not use any cell line.

    d. If any of the cell lines used are listed in the database of commonly misidentified cell lines maintained by ICLAC, provide a scientific rationale for their use.

        We did not use any cell line.

▶ Animals and human research participants

Policy information about studies involving animals; when reporting animal research, follow the ARRIVE guidelines

11. Description of research animals

Provide all relevant details on animals and/or animal-derived materials used in the study.

We used a C57BL/6; 129 mixed background mice in all the experiments, female and male mice were randomly allocated into different groups, mice were used in the age between 7 and 32 weeks' old. Detailed information in provided in the method section. All mice were used in accordance with the guidelines of the Institutional Animal Care and Use Committee of the Institute for Nutritional Sciences and Shanghai Institute of Biochemistry and Cell Biology, Shanghai Institute for Biological Sciences, Chines Academy of Sciences

Policy information about studies involving human research participants

12. Description of human research participants

Describe the covariate-relevant population characteristics of the human research participants.

There is no human subjects